



OPEN ACCESS

EDITED BY
Wen Zhuang,
Shandong University, China

REVIEWED BY
Liqin Duan,
Institute of Oceanology Chinese Academy
of Sciences, China
Ruifeng Zhang,
Shanghai Jiao Tong University, China

*CORRESPONDENCE
Jingling Ren
✉ renjingl@ouc.edu.cn

SPECIALTY SECTION
This article was submitted to
Marine Biogeochemistry,
a section of the journal
Frontiers in Marine Science

RECEIVED 21 December 2022

ACCEPTED 01 March 2023

PUBLISHED 17 March 2023

CITATION
Yang Y, Li L, Ren J, Jiang S and Zhang J
(2023) Processes controlling the
distributions and cycling of dissolved
aluminum and manganese in the
northeastern Indian Ocean.
Front. Mar. Sci. 10:1128657.
doi: 10.3389/fmars.2023.1128657

COPYRIGHT
© 2023 Yang, Li, Ren, Jiang and Zhang. This
is an open-access article distributed under
the terms of the [Creative Commons
Attribution License \(CC BY\)](https://creativecommons.org/licenses/by/4.0/). The use,
distribution or reproduction in other
forums is permitted, provided the original
author(s) and the copyright owner(s) are
credited and that the original publication in
this journal is cited, in accordance with
accepted academic practice. No use,
distribution or reproduction is permitted
which does not comply with these terms.

Processes controlling the distributions and cycling of dissolved aluminum and manganese in the northeastern Indian Ocean

Yichao Yang¹, Lei Li¹, Jingling Ren^{1,2*}, Shuo Jiang³
and Jing Zhang^{3,4}

¹Frontiers Science Centre for Deep Ocean Multispheres and Earth System, and Key Laboratory of Marine Chemistry Theory and Technology, Ministry of Education, Ocean University of China, Qingdao, China, ²Laboratory for Marine Ecology and Environmental Science, Qingdao National Laboratory for Marine Science and Technology, Qingdao, China, ³State Key Laboratory of Estuarine and Coastal Research, East China Normal University, Shanghai, China, ⁴School of Oceanography, Shanghai Jiao Tong University, Shanghai, China

Aluminum and manganese are both key parameters in the GEOTRACES program. Data on dissolved aluminum (dAl) and dissolved manganese (dMn) relative to their geochemical behavior remain limited in the northeastern Indian Ocean (IO; including the Bay of Bengal (BoB) and equatorial Indian Ocean (Eq. IO)). Seawater samples collected in the BoB and Eq. IO during the spring inter-monsoon period (7 March to 9 April) of 2017 were analyzed to investigate the behavior and main processes controlling the distributions of dAl and dMn in the northeastern IO. The average concentrations of dAl and dMn in the mixed layer of the BoB were 16.6 and 6.7 nM, respectively. A modified 1-D box-model equation was utilized to estimate the contributions of different sources to dAl and dMn in the mixed layer. Al released from the desorption of and/or dissolution of the lithogenic sediments discharged by the Ganga–Brahmaputra (G-B) river system predominantly controlled the dAl distributions in the mixed layer of the BoB, while the desorption from the lithogenic sediments only contributed approximately 13%–21% dMn. Additional dMn input from the advection of Andaman Sea water and photo-reduction–dissolution of particulate Mn(IV) contributed more than 60% dMn in the mixed layer of the BoB. dAl and dMn in the surface mixed layer of the Eq. IO were mainly affected by the mixing of dAl- and dMn-enriched BoB surface water and low-dAl, low-dMn southern Arabian Sea surface water. Considering water mass properties and dAl concentrations, the distributions of dAl in the intermediate water (750–1,500 m) of northeastern IO were controlled by the mixing of Red Sea Intermediate Water, Indonesian Intermediate Water, and intermediate water of the BoB. Different from dAl, the apparent oxygen utilization relationship with dMn concentrations indicated that the regeneration

of lithogenic particles under hypoxic conditions played a more important role than the remineralization of settling organic particles in controlling dMn distributions in the subsurface and intermediate water body (100–1,000 m) of the BoB and that remineralization of biogenic particles mattered to dMn in the subsurface of the Eq. IO.

KEYWORDS

dissolved aluminium, dissolved manganese, Indian Ocean, Bay of Bengal, influencing factors

Introduction

Aluminum (Al) and manganese (Mn) are considered key parameters in the GEOTRACES program (GEOTRACES Planning Group, 2006). Al is widely used as a tracer of atmospheric deposition to the ocean (Measures and Brown, 1996; Grand et al., 2015a). Mn is an essential micronutrient for photosynthesis and the normal function of enzymes in cells of phytoplankton (Gerringa et al., 2020). Furthermore, both Al and Mn can be used for tracing water masses mixing (Measures and Edmond, 1990; Statham et al., 1998; Zheng et al., 2022) and external sources, e.g., continental inputs (Slemons et al., 2010; Menzel Barraqueta et al., 2018; Kandel and Aguilar-Islas, 2021) and hydrothermal inputs (Resing et al., 2015; Lee et al., 2018). Mn is also used as a chemical tracer for understanding changes in the redox environment (Lenstra et al., 2020) in the ocean due to its variable valence.

Dissolved Al (dAl) is particle reactive, and its vertical profile typically presents a scavenged type in many ocean regions (Bruland et al., 2014), i.e., elevated concentrations in the surface and decreasing and keeping uniform concentrations in the deep ocean. Dissolved Mn (dMn) generally behaves as a scavenged type (Landing and Bruland, 1980; Colombo et al., 2020) but sometimes increases its concentration below the surface where dissolved oxygen is low (Thi Dieu Vu and Sohrin, 2013; Lenstra et al., 2020). Different from dAl, the elevated concentration of dMn in the surface layer mainly results from the photo-reduction-dissolution of Mn oxides (Sunda and Huntsman, 1994; Hood et al., 2009). Atmospheric deposition (Baker et al., 2006; Hsu et al., 2010; Kadko et al., 2020), hydrothermal venting (Resing et al., 2015; Chen and Wu, 2019), sediment resuspension (Wang et al., 2018; Colombo et al., 2022), and fluvial input (dissolved species and lithogenic release; Aguilar-Islas and Bruland, 2006; Singh et al., 2020) are all the main sources of dAl and dMn in the ocean. Moreover, Mn can transfer its valence from particle Mn(IV) to dissolvable Mn(II) by reductive dissolution and enter the water body below the surface layer (Lee et al., 2018; Lenstra et al., 2020; Colombo et al., 2022). Both dAl and dMn concentrations have shown huge inter-oceanic distinctions due to different biogeochemical behavior and external sources in different oceanic basins (Obata et al., 2004; Thi Dieu Vu and Sohrin, 2013; Rolison et al., 2015; Grand et al., 2015b; Häusler et al., 2018; Menzel

Barraqueta et al., 2018; Wang et al., 2018; Nakaguchi et al., 2021; Singh and Singh, 2022). The concentration of dAl varies in a large range (0.05 to 673.4 nM; Menzel Barraqueta et al., 2020) in the global ocean, while dMn shows a relatively small concentration range (0.1 to 25 nM; Shiller, 1997).

The Indian Ocean (IO) occupies approximately one-fifth of the world's ocean net primary production (Behrenfeld and Falkowski, 1997) and is characterized by seasonal reversal of monsoonal winds and surface currents (Shankar et al., 2002). The IO is one of the least understood oceans due to its physical and biogeochemical dynamics (Hood et al., 2009). Obata et al. (2004) determined the vertical profiles of dAl and other elements in several stations in eastern IO. Thi Dieu Vu and Sohrin (2013) reported the basin-scale distribution of dAl, dMn, and other trace elements in the IO. Singh and Singh (2022) studied dAl distributions over the full vertical water column profiles in the Arabian Sea and the western equatorial IO. Data on dAl and dMn relative to their biogeochemical behavior remain limited in the northeastern IO. Grand et al. (2015b) conducted a meridional study from the Indian sector of the Southern Ocean to the Bay of Bengal (BoB) spaced at approximately 1° intervals, focusing on the distribution of dAl and dissolved Fe. The atmospheric dry deposition was investigated simultaneously (Grand et al., 2015a). Singh et al. (2020) measured dAl from the subtropical gyre region to the northern IO, including the BoB, the Andaman Sea, and the Arabian Sea. The huge continental input, in the form of freshwater, suspended sediments, and atmospheric deposition, deeply influence the biogeochemistry of lithogenic trace metals (e.g., Al and Mn) in the BoB and equatorial IO (Sengupta et al., 2006; Srinivas and Sarin, 2013). Moreover, due to the large riverine freshwater input, excessive rainfall, and strong stratification, along with the oldest central water in the north IO, the BoB is one of the four anoxic areas in the global ocean (Kamykowski and Zentara, 1990; You and Tomczak, 1993). Therefore, to better understand and assess the effect of different processes on the biogeochemistry of northeastern IO, we report the continental input and redox tracer, i.e., dAl and dMn concentrations in the BoB and equatorial IO during the spring inter-monsoon period (7 March to 9 April) in 2017. In this study, a modified 1-D model equation, T-S diagram, and correlations between dAl, dMn, and relevant hydrographic parameters are used to figure out the principal sources and processes governing dAl and dMn distributions in the northeastern Indian Ocean and

add to the comprehensive understanding of dAl and dMn behavior in the anoxic ocean.

Materials and methods

Study area and sampling

The BoB covers an area of 2.2×10^6 km², with an average depth of 3 km (Singh et al., 2012). The Ganga and Brahmaputra rivers together discharge 1,050 km³/year of water, which could extend to 8°S (Nath et al., 1989), and approximately one billion tons of sediments (Galy and France-Lanord, 2001) to the BoB. Unger et al. (2003) conducted sediment trap experiments in the BoB and found obvious seasonal and interannual variations in fluxes of river sediments. The surface water of the northeastern IO receives dust input from the Indian plains, Southeast Asia, combined with possible long-range inputs from the Thar Desert (Srinivas et al., 2012; Srinivas and Sarin, 2013). Moreover, the Indonesian Throughflow (ITF) carries warm and low-salinity surface water from the west Pacific Ocean into the east IO (Gordon, 2005), and the South Equatorial Current (SEC) carries the ITF westward (You, 1998).

Seawater samples were collected aboard the *R/V ShiYan 3* in the northeastern IO during the spring inter-monsoon period (7 March to 9 April) of 2017. The dataset encompassed a total of 50 stations (Figure 1), including 37 surface stations (~10 m), eight stations of upper 500 m, and five full vertical profiles. The layer number of vertical profiles was determined as 7–8 for stations of upper 500 m and as 14–20 for the full ones, according to the water mass properties obtained from the down cast reading of temperature and salinity from the conductivity, temperature, and depth (CTD) sensor at each station. All samples were obtained through an X-Vane sampler, which consisted of a 5-L Niskin-X sampling bottle attached to a titanium and polyvinyl chloride (PVC) polymer supporting frame (“II-style” secure assembly) (Zhang et al., 2015b). The X-Vane sampler controls the Niskin-X bottle upstream of the hydrowire, away from the contaminations of the hydrowire and ship. Once the sampling bottle arrives at the desired depth, the Teflon-coated messenger is used to strike the “II-style” assembly and close the Niskin-X bottle to obtain a clean seawater sample. Five-liter Niskin-X bottles were washed rigorously according to the GEOTRACES cookbook (using Citranox (Alconox, White Plains, NY, USA), Milli-Q water (Advantage 10, Millipore, Burlington, MA, USA), 10% HCl (purified by quadruple sub-boiling point distillation in a quartz glass still) leaching solution, and Milli-Q water in sequence) and sealed using double plastic bags according to Zhang et al. (2015b). The low-density polyethylene (LDPE) and high-density polyethylene (HDPE) bottles (Nalgene, Rochester, NY, USA) and perfluoroalkoxy alkane (Savillex, Eden Prairie, MN, USA) filtration assemblies were cleaned using 2 M of purified HCl, ~1 M of Purified HCl, and Milli-Q water in sequence in a class-1000 clean lab at East China Normal University according to Zhang et al. (2015a). Samples for dissolved measurements once recovered were then taken directly to a class-100 portable clean bench (Air Control) using the filtration system and washed using the same procedures. Filtration was immediately carried out through a 0.4- μ m, acid-washed, 47-mm polycarbonate membrane

(Whatman, Kent, UK) in a class-100 clean bench. Subsamples were collected in 250-ml Nalgene LDPE bottles, double bagged, and quickly frozen at –20°C. Blank experiments were also carried out using Milli-Q water that was filtrated under the same conditions for the investigation of the contamination.

Analysis of dissolved Al and Mn

Frozen samples were sufficiently thawed and then acidified to pH 1.7 using purified HCl. dAl and dMn concentrations were determined at approximately 1 h after acidification. The dissolved Al was determined using the online preconcentration flow injection analysis (FIA) method modified from Brown and Bruland (2008). Briefly, the main modification was loading the buffered sample onto the column directly without conditioning the column buffer. The determining blank with its variation and the result of reference sample determination were satisfying (see below). The dissolved Mn samples were analyzed using the FIA method developed by Aguilar-Islas and Bruland (2006) in the lab. The detection limit, defined as three times the standard deviation of the blank, was 0.18 nM for Al (n = 9) and 0.21 nM for Mn (n = 9). The precision of the measurements of dAl and dMn was below 2% when concentration was high (dAl, 20 nM; dMn, 8 nM; n = 11) and below 5% for low concentration (dAl, 5 nM; dMn, 1 nM; n = 11). The column-cleaned low background seawater was made by passing buffered South China Sea seawater through the preconcentration column (Nobias Chelate PA-1, Hitachi, Japan) for estimation of the procedural blank during the sample analysis.

Multiple reference seawater samples, including Canada Standard Reference Seawater (NASS-6), North Atlantic GEOTRACES reference standards (GEOTRACES GS and GEOTRACES GD), and North Pacific reference standards (SAFE-S), were analyzed for dAl and dMn concentrations. Results of dAl and dMn measurements for the abovementioned reference seawater samples had no significant difference with consensus value (Table 1, *t*-test, *p* > 0.01).

A 1-D box-model equation to estimate external source contribution

A modified version of the 1-D box-model equation proposed by Grand et al. (2015a) was utilized to estimate the dAl and dMn input to the mixed layer, originating from atmospheric deposition and/or fluvial sediment discharge to the BoB and the equatorial Indian Ocean (Eq. IO). The 1-D box-model equation is given as follows:

$$dM = \frac{G \times MRT \times f_M \times Sol.}{M_{wt} \times MLD_c} \times 10^6, \quad (1)$$

where *dM* is the concentration of dissolved trace metals (in nM), *G* represents the lithogenic sediment flux (in g/(m²·year)), *MRT* is the mean residence time (in years) of trace metals in the mixed layer, *f_M* is the fraction of trace metals in the particles (including sediments and aerosols), *Sol.* is the fractional solubility of trace metals from the lithogenic sediments or atmospheric dust,

TABLE 1 Comparison of measured dAl (nM) and dMn (nM) concentrations (this study) and consensus values in SAFe and GEOTRACES reference samples (n = 3).

Reference sample	Al		Mn	
	Consensus value	This study	Consensus value	This study
NASS-6	–	–	9.4 ± 0.5	9.6 ± 0.9
GEOTRACES GS	27.5 ± 0.2	27.2 ± 0.3	1.62 ± 0.15	1.50 ± 0.11
GEOTRACES GD	17.7 ± 0.2	18.0 ± 0.7	–	0.21 ± 0.03
SAFe-S	1.67 ± 0.1	1.60 ± 0.2	0.82 ± 0.08	0.79 ± 0.06

dAl, dissolved aluminum; dMn, dissolved manganese. –, No available data.

M_{wt} is the atomic weight of trace metals (in g/mol), MLD_c (in m) is the depth of mixed layer retrieved from a density based on our own CTD calculated density of the sampling locations (data in accordance with Holte et al. (2017)), and 10^6 is the factor of conversions of units.

Results

The hydrographical setting

Several studies have discussed the circulation and the structure of water masses in the IO (Shankar et al., 2002; Schott et al., 2009; Singh et al., 2012). The study area (Figure 1) is separated into two sub-basins for the convenience of discussion: 1) the BoB (north of 5°N, 80–92°E) and 2) Eq. IO [5°S–5°N, including station I507 (6.5° S, 98.3°E)]. From the data obtained, salinity on the surface was higher in the south and west and lower in the north and east (Figure 2B). Station I201, which was influenced by not only South Asian Subcontinent fluvial input but also the outflow of the Andaman Sea, possessed the lowest salinity (32.43) with a relatively low temperature (29.6°C). Relatively low salinity (33.52) and temperature (28.6°C) were observed at the southeastmost station I507 compared to nearby stations. The abnormally high salinity was also found at station I103. In section E, the zonal distribution of salinity showed a decreasing trend from west to east, and a high-salinity (~35.5) water tongue appeared in the subsurface (60–120 m) (Figure 3A). Dissolved oxygen (DO) was in the range of 47 to 78 μM under the subsurface of section E (except for station I415). In the whole section L, DO was lower than 63 μM in the depth range from 200 to 1,250 m (Figure 4B). In the BoB, DO reached its minimum (<16 μM) below the pycnocline, while DO below the surface of the Eq. IO was in the range of 31 to 78 μM, slightly higher than that in the BoB.

The T-S diagram (Figure 5) suggested major source water masses in this study. The tremendous Ganga–Brahmaputra (G-B) River System freshwater and local excess of precipitation over evaporation leads to the formation of Bay of Bengal Water (BBW), which was characterized by low salinity (32.43–33.48, observed in this study) and high dAl and dMn (12.3–19.9 and 5.1–8.7 nM, respectively). In addition, the Andaman Sea is also characterized by the low salinity for receiving freshwater from Irrawaddy and Salween rivers. Low-salinity surface water of the Andaman Sea may be transported to the

BoB as well (Singh et al., 2020). The Equatorial Counter Current (ECC) carries Arabian Sea High-Salinity Water (ASHSW), which was characterized by high salinity and relatively low dAl and dMn (I401, salinity = 34.96, dAl = 4.3 nM, and dMn = 1.0 nM, this study; ER-8, salinity = 35.48, dAl = 3.0 nM, and dMn = 1.4 nM, Thi Dieu Vu and Sohrin, 2013) eastward to the east Eq. IO. Meanwhile, the BBW is able to spread southward to the east Eq. IO (I407–I415, salinity ~ 34.00, Figures 2B, 3A; Sandeep et al., 2018) as well. The existence of BBW leads to strong stratification and inhibits vertical mixing in the BoB. The low-salinity BBW overlies North Indian Central Water (NICW), which is aged from Indian Central Water (ICW) and occupies a major subsurface water body in the north IO (You, 1997). NICW is the oldest central water of the north IO (You and Tomczak, 1993) and becomes depleted in oxygen (<25 μM, Figure 4B). The concentrations of dAl and dMn were relatively high (dAl = 6.7 ± 4.3 (1SD) nM, dMn = 2.7 ± 1.7 (1SD) nM) in ICW and NICW. The potential temperature and

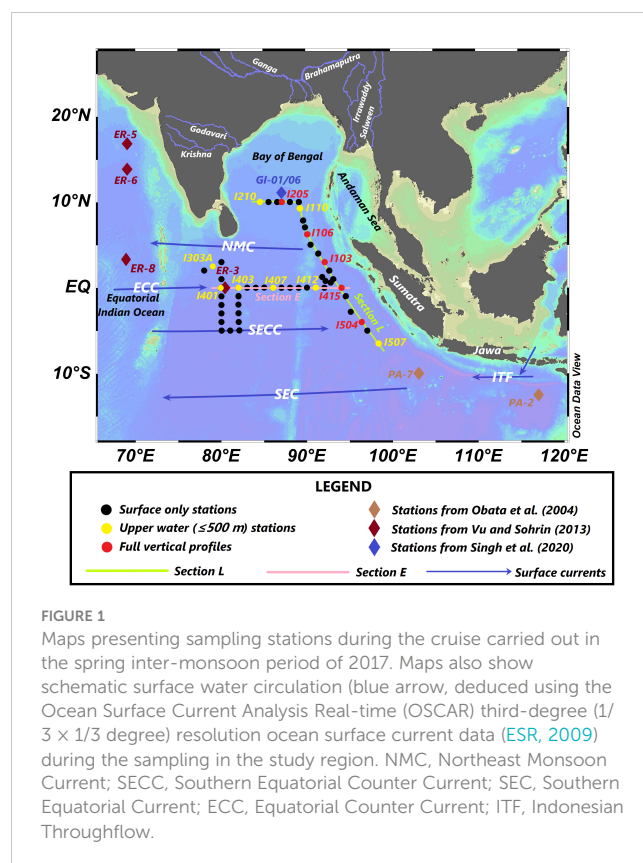


FIGURE 1 Maps presenting sampling stations during the cruise carried out in the spring inter-monsoon period of 2017. Maps also show schematic surface water circulation (blue arrow, deduced using the Ocean Surface Current Analysis Real-time (OSCAR) third-degree (1/3 × 1/3 degree) resolution ocean surface current data (ESR, 2009) during the sampling in the study region. NMC, Northeast Monsoon Current; SECC, Southern Equatorial Counter Current; SEC, Southern Equatorial Current; ECC, Equatorial Counter Current; ITF, Indonesian Throughflow.

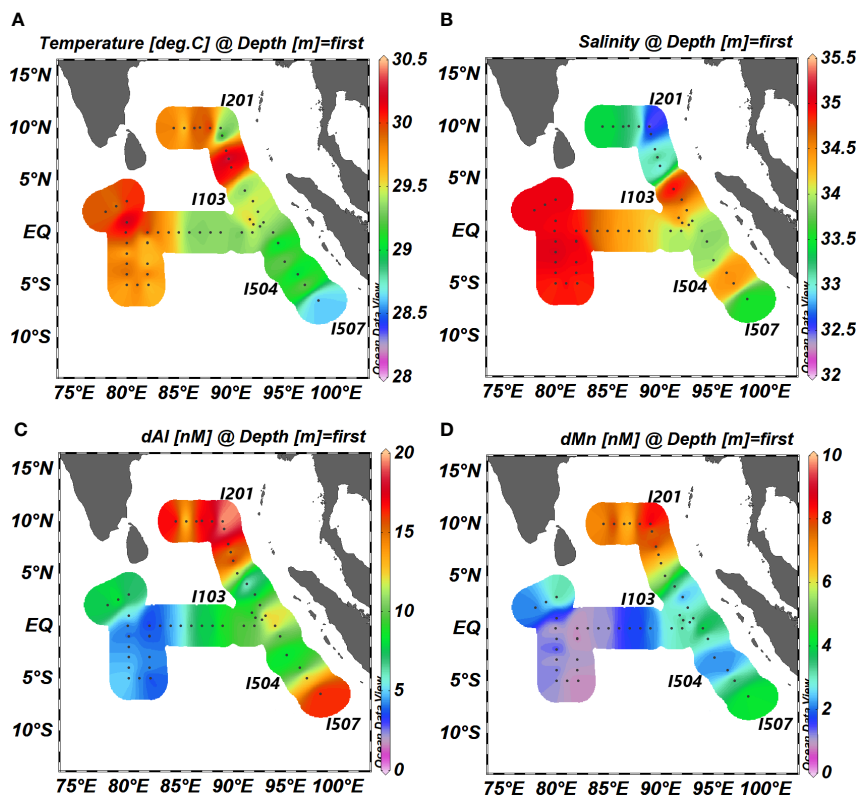


FIGURE 2 Horizontal distributions of (A) temperature, (B) salinity, (C) dAl, and (D) dMn in the surface of the northeastern IO. dAl, dissolved aluminum; dMn, dissolved manganese; IO, Indian Ocean.

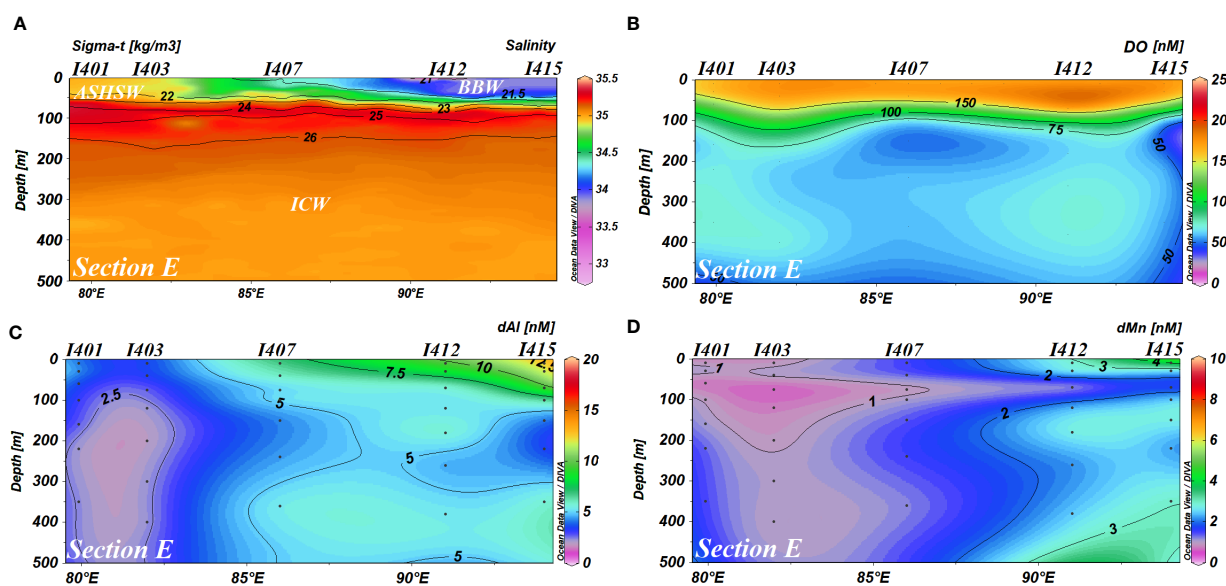


FIGURE 3 (A) Salinity, (B) DO, (C) dAl concentrations, and (D) dMn concentrations in the water column of section E DO, dissolved oxygen; dAl, dissolved aluminum; dMn, dissolved manganese.

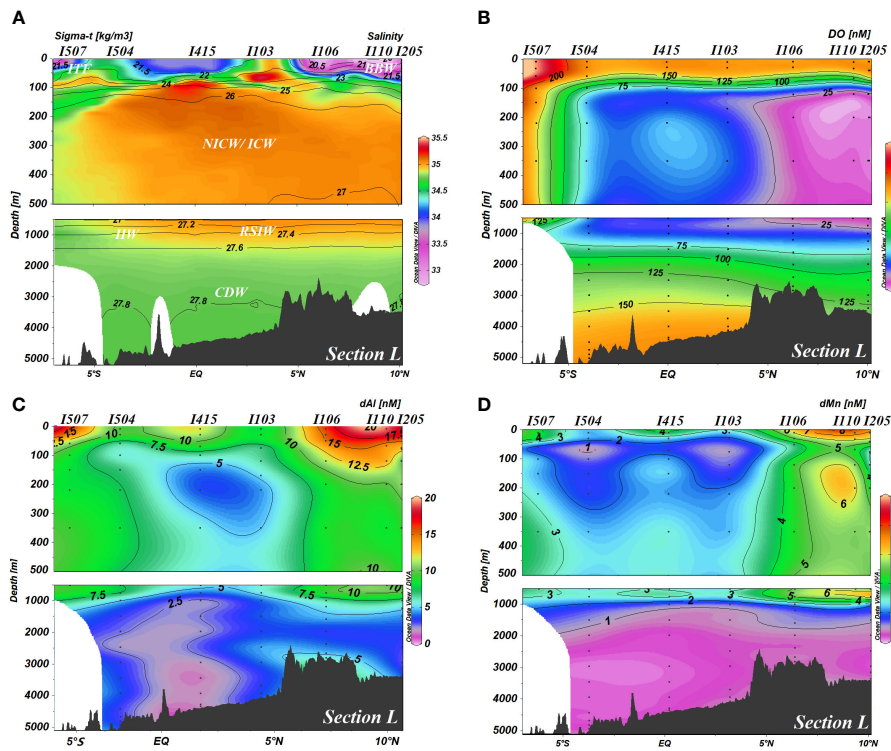


FIGURE 4 (A) Salinity, (B) DO, (C) dAl concentrations, and (D) dMn concentrations in the water column of section L. For better visualization of data, these four parameters' distributions are shown separately for the upper 500-m water column and the remaining water column (>500 m). DO, dissolved oxygen; dAl, dissolved aluminum; dMn, dissolved manganese.

salinity of intermediate water body in this study (σ_0 in the range of 27.1–27.6 kg/m³, depth within 750–1,500 m) are ~6.1°C–6.7°C and ~34.87–34.95, respectively. The intermediate water body of the study area is mainly from two water masses, i.e., Red Sea Intermediate Water (RSIW; θ ~ 8.2–12.0°C, salinity ~ 35.37–35.63, You, 1998) and Indonesian Intermediate Water (IIW; θ ~ 4.7–8.2°C, salinity ~ 34.63–34.69, You, 1998) through T-S diagram.

Horizontal distributions of dissolved Al and Mn in the northeastern IO

The differences between the average value of concentrations in the mixed layer (20–30 m in the BoB, 30–35 m in the Eq. IO; dAl = 9.7 ± 5.0 (1SD) nM, dMn = 3.2 ± 2.3 (1SD) nM, n = 62) and surface layer (10 m; dAl = 9.2 ± 4.8 (1SD) nM, dMn = 3.2 ± 2.4 (1SD) nM, n = 50)

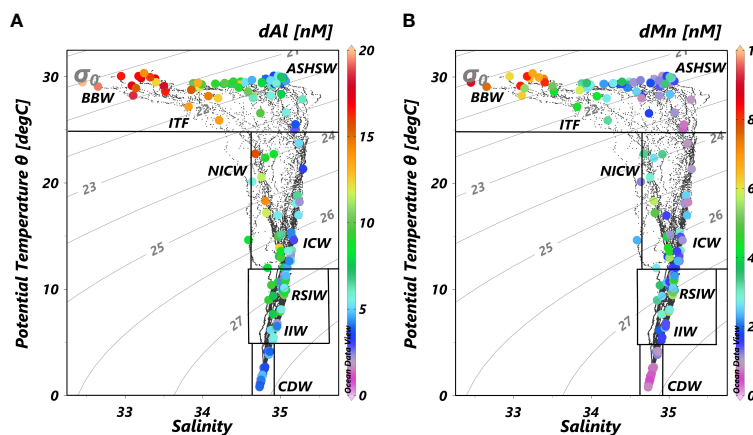


FIGURE 5 T-S diagrams of (A) dissolved Al and (B) dissolved Mn concentrations from stations in the northeastern IO. The gray solid curves were isopycnals with σ_0 values (kg/m³) denoted. The definitions of different water masses were based on You (1997); You (1998), You (2000), Lewis and Luther III (2000), Sardessai et al. (2010), and Grand et al. (2015b). BBW, Bay of Bengal Water; ASHSW, Arabian Sea High Salinity Water; ICW, Indian Central Water; NICW, North Indian Central Water; IIW, Indonesia Intermediate Water; RSIW, Red Sea Intermediate Water; CDW, Circumpolar Deep Water.

were both within 10% for dAl and dMn in this study, indicating that the differences of concentrations of dAl and dMn were not significant between the surface layer and mixed layer in the study area. The distributions of dAl and dMn in the northern IO showed an increase from south to north and from west to east (Figures 2C, D). Station I201 possessed the highest dAl and dMn concentrations (19.9 and 8.7 nM, respectively) in the whole study area. Relatively high values of dAl and dMn (16.4 and 4.2 nM, respectively) were observed at the southeastmost station I507 compared to nearby stations. The abnormal low dAl and dMn were found at station I103, which will be discussed in the following section.

The dAl and dMn concentrations in the surface layer of the BoB were in the range of 12.3–19.9 and 6.1–8.7 nM, respectively. The mean dAl (16.7 ± 2.2 nM, $n = 10$) in the surface layer of the BoB in this study was comparable to that of PA-9 (14.7 nM, 8.00°N, 89.00°E, Obata et al., 2004) and was one- to twofold lower than the results from Singh et al. (9.2–48.3 nM, 2020). The northernmost station of Singh et al. (2020) was located at 20°N, 10° north of our station, indicating that the relatively high dAl concentration may come from the influence of freshwater input from the G-B River System. The ranges of dAl and dMn concentrations observed in the surface layer of the Eq. IO were 3.5–13.2 and 0.8–5.6 nM, respectively. The results of dAl and dMn were comparable to those of Singh et al. (2.5–15.4 nM, 2020) and Twining et al. (2.0–3.2 nM, 2019), respectively.

Vertical distributions of dissolved Al and Mn in the northern Indian Ocean

In section E, zonal distributions of dAl and dMn showed an increasing trend along with a decrease in salinity from west to east (Figure 3). A water tongue characterized by low dAl and dMn concentrations (<7.5 and <2 nM, respectively) appeared in the subsurface of section E, where dMn met its minimum value (<1 nM) at ~75 m. Both dAl and dMn in section E normally showed scavenging-type vertical profiles, i.e., enrichment in the surface water and decreasing with increasing depth. dMn in station I415 showed subsurface enrichment (~3 nM) at depths of 350 and 500 m.

In whole section L, distributions of dAl and dMn were regional discrepancies with DO (Figure 4). In the BoB, dAl exceeded 7.5 nM, even up to 12, and dMn could reach 6 nM, approaching the surface value. dAl and dMn concentrations were lower than 7.5 and 3 nM, respectively, in the Eq. IO. A similar distribution pattern between dAl and dMn was evident in the range of 500 to 1,000 m in section L, namely, maximum (dAl and dMn reaching up to ~10 and ~6 nM, respectively) in the BoB and minimum (dAl ~ 5 nM, dMn ~ 3 nM) in the Eq. IO. Both dAl and dMn concentrations showed remarkably uniform distributions below 1,000 m, which were consistent with the results of Singh et al. (2020) and Obata et al. (2004). The mean dAl concentration in the BoB was 4.7 nM, and an increasing dAl concentration (5.7 nM in station I106) toward the seafloor was observed. Simultaneously, in the Eq. IO, the mean dAl concentration was 3 nM below 1,000 m, lower than that in the BoB. dMn concentration was lower than 2 nM below 1,000 m, and the

mean values were 0.9 and 0.5 nM in the BoB and the Eq. IO, respectively.

Discussion

Validation of dAl and dMn data with published results

Indian GEOTRACES station, GI-01/06 (11.01°N, 87.00°E, sampled in March 2014, Singh et al., 2020) in the BoB, was 112 km north of station I205 (10.00°N, 87.00°E, sampled in March 2017) in this study (Figure 1). Both stations were sampled during the spring inter-monsoon period. The dAl concentrations had significant differences (*t*-test, $p < 0.05$) in the upper 1,000 m but mostly overlapped in the deeper water (>1,000 m) (Figure 6A). Considering the long time span (3 years) between occupations of two stations, these differences may be attributed to variations of G-B River System freshwater discharge and lithogenic sediment fluxes to the BoB (Unger et al., 2003), which predominantly control the dissolved Fe (Chinni et al., 2019) and dAl (Singh et al., 2020) distributions, and will be discussed later in Section 4.2.

Japanese GEOTRACES station, ER-3 (0°, 80°E, sampled in November 2011, Thi Dieu Vu and Sohrin, 2013), almost overlaps station I401 (0.01°S, 79.92°E) (Figure 1). Salinity at two stations had significant differences (*t*-test, $p < 0.05$) in the upper water column (<200 m), and Mn distributions showed a significant difference in the upper 500 m water body (*t*-test, $p < 0.05$, Figure 6B). The northeastern IO is characterized by the seasonal reversal of monsoonal winds and surface currents (Shankar et al., 2002). ER-3 was sampled in November 2009, while I401 was in March 2017. March is the first month of the end of the Northeast Monsoon. The Northeast Monsoon Current carries fresher BoB water into the Arabian Sea. November is the first month of the start of the Northeast Monsoon, and the currents still exist but feature the Southwest Monsoon Current, which flows eastward from the Arabian Sea to the BoB (Shankar et al., 2002; Schott et al., 2009). Currents flowing differently and interannual differences contributed to significant differences in salinity and dMn concentrations in the depth of upper 500 m. Such difference was also observed above 1,000 m when full vertical profile station I415 was compared with station ER-3. dMn showed more sensitivity toward seasonal variations than dAl because dMn was not only seriously affected by riverine inputs (Aguilar-Islas and Bruland, 2006) but also influenced by ambient oxidation conditions (Lenstra et al., 2020). High dMn concentration in the BoB subsurface layer caused by regeneration under a low oxygen environment and the water mass mixing resulted in a relatively high dMn value in station I415 than that of ER-3 in the upper 1,000 m water body. Although the two stations were 12 longitudes apart, dMn concentrations showed comparable results in the deeper waters (>1,500 m). In general, dAl and dMn concentrations showed variations on account of different sampling seasons and years in the upper water column (<1,000 m) at nearby stations and were comparable in the deep water. The factors that may influence dAl and dMn distributions in different areas and water depths are discussed in the following section.

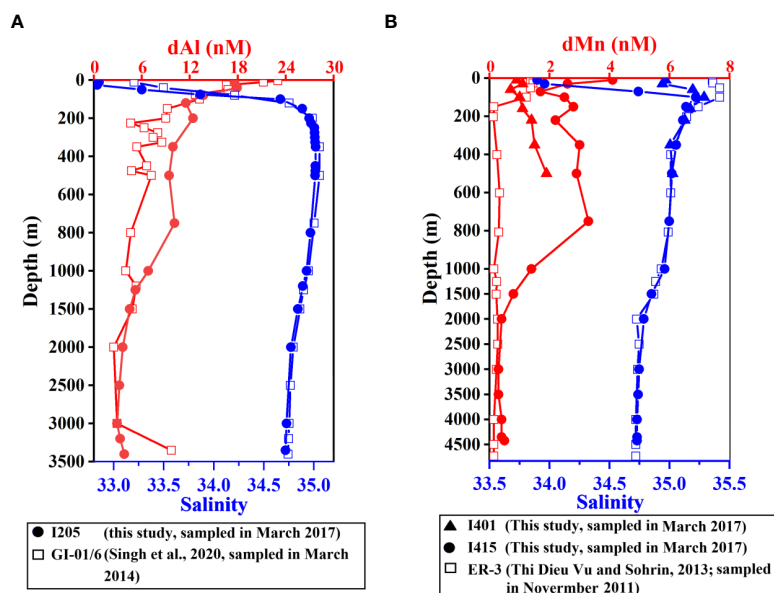


FIGURE 6

(A) Comparisons of salinity (blue) and dAl (red) at the full vertical profile of dAl of Indian GEOTRACES stations GI-01/06 (hollow square, Singh et al., 2020) and I205 (dot, this study). (B) Comparisons of salinity (blue) and dMn (red) at Japanese GEOTRACES stations ER-3 (hollow square, Thi Dieu Vu and Sohrin, 2013), I401 (triangle, this study), and I415 (dot, this study). dAl, dissolved aluminum; dMn, dissolved manganese.

Potential external sources of the mixed layer of BoB

Tremendous fluvial input (including freshwater and lithogenic sediments), along with atmospheric deposition and its subsequent dissolution, plays significant roles in regulating the dAl and dMn distributions in the BoB. Therefore, the 1-D box-model Equation 1 was used to estimate potential sources of dAl and dMn in the mixed layer of the BoB. As shown in Table 2; Grand et al. (2015a) calculated the residence time of dAl in the surface mixed layer to be 1.1 years in the northeastern IO (north of 5°S), while 0.01–0.47 years in the Arabian Sea was given by Singh and Singh (2022). The residence time of dMn varies in different areas (Table 2). For consistency, the same Al residence time (i.e., 1.1 years) and the mean value of Mn residence time of other studies (i.e., 1.0 years) were used to calculate different source contributions.

Mn was categorized as a crustal-derived element, same as Al (Hsu et al., 2010), while the solubility of the two elements differed (Table 2). The solubility of dAl used in the study was chosen as 3.6%, the same as that of Grand et al. (2015a) and Singh et al. (2020). The solubility of Mn from atmospheric dust was all relatively high in different areas and was chosen as 50%. Atmospheric Al dry deposition flux ($0.3 \text{ mg Al}\cdot\text{m}^{-2}\cdot\text{day}^{-1}$; Srinivas and Sarin, 2013) over the south BoB was chosen to calculate the atmospheric deposition of Al. After substituting all parameters above into Equation (1), the estimate of dust input supported dAl in the south BoB was found to be 1.8–2.7 nM. Similarly, $7.8 \mu\text{g Mn}\cdot\text{m}^{-2}\cdot\text{day}^{-1}$ (Srinivas and Sarin, 2013) was used, and the results showed that approximately 0.3–0.4 nM of dMn was contributed by atmospheric deposition to the mixed layer of the BoB.

The average concentration of dAl of the G-B River System was taken as 57 nM (salinity ≈ 29.4 , Singh et al., 2020). Grand et al. (2015a) and Singh et al. (2020) both found that mixed layer dAl and salinity were negatively correlated in the BoB where salinity > 31 . Based on the riverine freshwater charge ($1,300 \text{ km}^3/\text{year}$, Sengupta et al., 2006), the area of the BoB ($2.2 \times 10^{12} \text{ m}^2$, Singh et al., 2020), and an average depth of mixed layer (20–30 m, this study), 1.3–1.9 nM enrichment of dAl in the mixed layer of the BoB was calculated due to discharge of the G-B River System. Relatively few studies focused on the distribution of dMn in the BoB nowadays. The value of 20 nM was chosen as the endmember of riverine freshwater input for dMn (unpublished data, measured at the G-B river estuary), and 0.2–0.4 nM of dMn was calculated from the G-B river system contributing to the BoB.

Singh et al. (2020) estimated the Al fraction in the sediment input to the BoB to be 8% by weight, which was similar to the Al composition in the upper continental crust (8.04%, Taylor and McLennan, 1985) and the suspended sediments of Brahmaputra River (7.9%, Singh and France-Lanord, 2002). The Mn composition by weight was 673 ppm in the suspended sediments of the Brahmaputra River (Singh and France-Lanord, 2002) and 600 ppm in the upper crust (Taylor and McLennan, 1985). The same Al concentration (8%) and Mn (650 ppm by weight) were used to calculate sediment input to the BoB. The solubility of Al from lithogenic sediments was chosen as 2.4% referring to Singh et al. (2020). Considering the atmospheric mineral dust to be originating from the upper crust and the results from Tessier et al. (1979) that labile particulate species occupied the percentage of total particulate concentration through five fractions processed, the solubility of Mn in the lithogenic sediments was assumed to be 50%. Substituting lithogenic sediment load (sediment trap in the south BoB, 4.3

TABLE 2 Values of each parameter chosen in the BoB.

Area		Pacific Ocean	East China Sea	Atlantic Ocean	South Pacific Ocean*	Bay of Bengal	South China Sea**	North Pacific Ocean***	Arabian Sea	Value chosen in this study
Sol. (%)	Al	3.7	5–10	4.1 ± 3.9		3.6				3.6
	Mn	45.1	50	52.9 ± 31.1	35.9 ± 11.9					50
MRT (year)	Al					1.1 ± 0.8			0.01–0.47	1.1
	Mn				0.73 ± 0.1		1.4–5.2	0.22–1.8		1.0
Reference		Buck et al., 2013	Hsu et al., 2010	López-García et al., 2017	Kadko et al., 2020	Grand et al., 2015a	Wang et al., 2018	Martin and Knauer, 1980	Singh and Singh, 2022	

* From coast to open ocean in the south Pacific Ocean.

** The mixed layer of the South China Sea.

*** The depth of 1–150 m of the central north Pacific Ocean.

$\text{g}\cdot\text{m}^{-2}\cdot\text{year}^{-1}$, Unger et al., 2003) into Equation (1), dAl released in the mixed water of the south BoB from the sediments was estimated to be 11.2–16.8 nM. This estimated Al release from suspended sediment was an order magnitude larger than that from G-B river freshwater (1.3–1.9 nM). dMn from lithogenic sediment release was in the range of 0.9 to 1.4 nM.

Al released from lithogenic sediments predominately controlled the concentration of dAl (16.6 nM, average value), accounting for more than 67% of bulk inventory, and freshwater discharge played a secondary role in intense scavenging at the estuary. Atmospheric Al dry deposition contributed approximately 14% dAl in the mixed layer of the south BoB. There was no correlation between dAl and dMn ($r = 0.02$, Figure 7, right) in the mixed layer of the south BoB, indicating different controlling processes of dAl and dMn. Each source accounted for dMn (6.7 nM, average value) differed from that of dAl. Lithogenic sediments release supported only approximately 13%–21% dMn. Both freshwater input and

atmospheric Mn dry deposition input contributed ~5% dMn. The three aforementioned sources sustained ~33% dMn in the mixed layer of the BoB at most. Additional dMn input from the advection of dMn-rich, low-salinity surface waters from the Andaman Sea may be another significant source (Singh et al., 2020). Moreover, numerous insoluble Mn(IV) oxides could be converted into dissolved Mn(II) for photo-reduction (Sunda and Huntsman, 1994). Meanwhile, a high dissolution efficiency of dust-derived Mn resulting from photochemical reduction was also observed by Sunda and Huntsman (1988) and Thi Dieu Vu and Sohrin (2013), indicating another important source for dMn in the surface seawater.

The range of different source contributions above was mainly from the indeterminacy of mixed layer depth. Other variable parameters could also cause uncertainties in the contribution calculation. For example, the G-B River System discharge used in this study was $1,300 \text{ km}^3/\text{year}$ and had existing 13% interannual

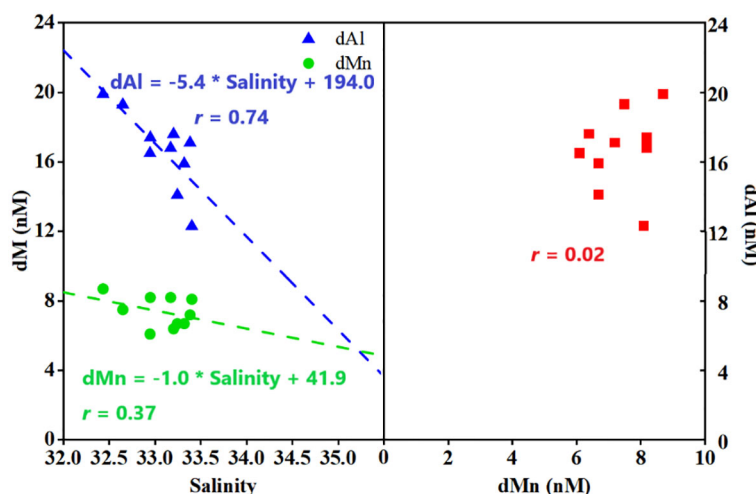


FIGURE 7 dAl and dMn variations with salinity in the mixed layer for stations in BoB (left). dMn variation with dAl in the mixed layer of BoB (right). dAl, dissolved aluminum; dMn, dissolved manganese; BoB, Bay of Bengal.

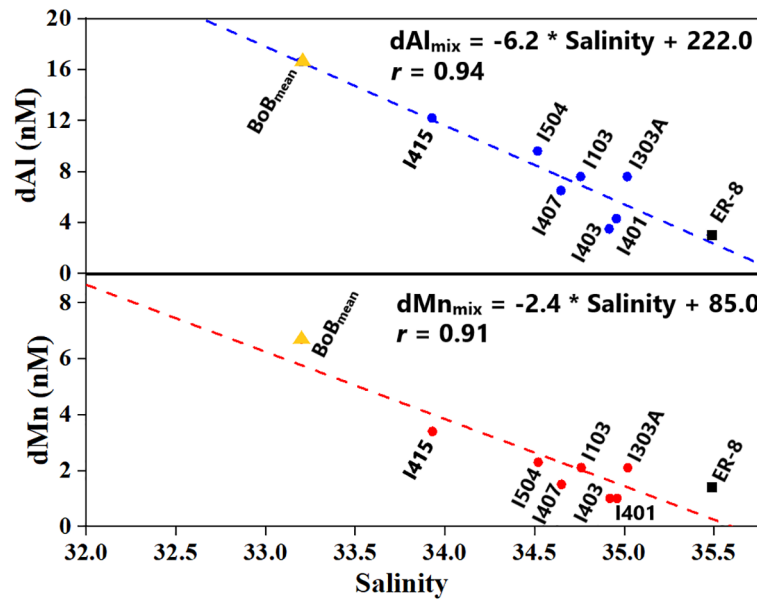


FIGURE 8

dAl (up) and dMn (down) variations with salinity for the mixed layer of stations in the Eq. IO (all stations located in 5°S–5°N). Data point for BoB_{mean} was the average value in the mixed layer of south BoB. Data point for station ER-8 (4.02°N, 69.00°W, Thi Dieu Vu and Sohrin, 2013) in the southern Arabian Sea was also plotted as an endmember. dAl, dissolved aluminum; dMn, dissolved manganese; Eq. IO, equatorial Indian Ocean; BoB, Bay of Bengal.

variations (Dai and Trenberth, 2002; Jian et al., 2009), bringing 13% contribution calculation result uncertainty. Nevertheless, even if considering this uncertainty, lithogenic sediment release may still play a predominant role in dAl distributions in the mixed layer of the BoB. Unlike dAl, sources other than lithogenic sediments were of great importance in controlling dMn contributions.

Water mass mixing in the northeastern IO

Significant low dAl and dMn concentrations compared to the nearby stations were observed at stations I103 and I504, accompanied by high salinity and low temperature (Figure 2). An upwelling isopycnal, which the two stations possessed (Figure 4A),

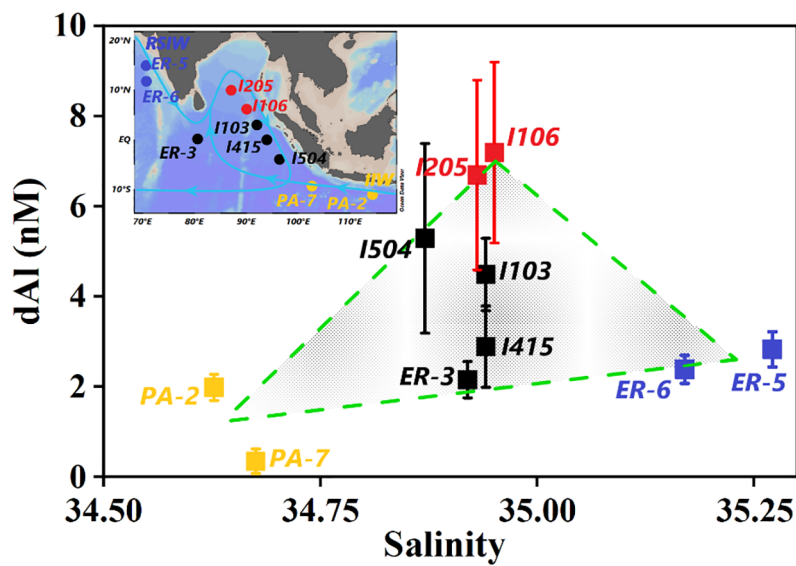


FIGURE 9

dAl variation with salinity for σ_0 within 27.1–27.6 kg/m³ from stations in this study. ER-3, ER-5, and ER-6 from Thi Dieu Vu and Sohrin (2013) and PA-2 and PA-7 from Obata et al. (2004). The error bar means the range of dAl concentration. The inset map shows the locations of stations ahead, and the light blue line represents intermediate water (σ_0 within 27.1–27.6 kg/m³) circulation pattern in the northeastern IO (adapted from You, 1998). dAl, dissolved aluminum; BoB, Bay of Bengal.

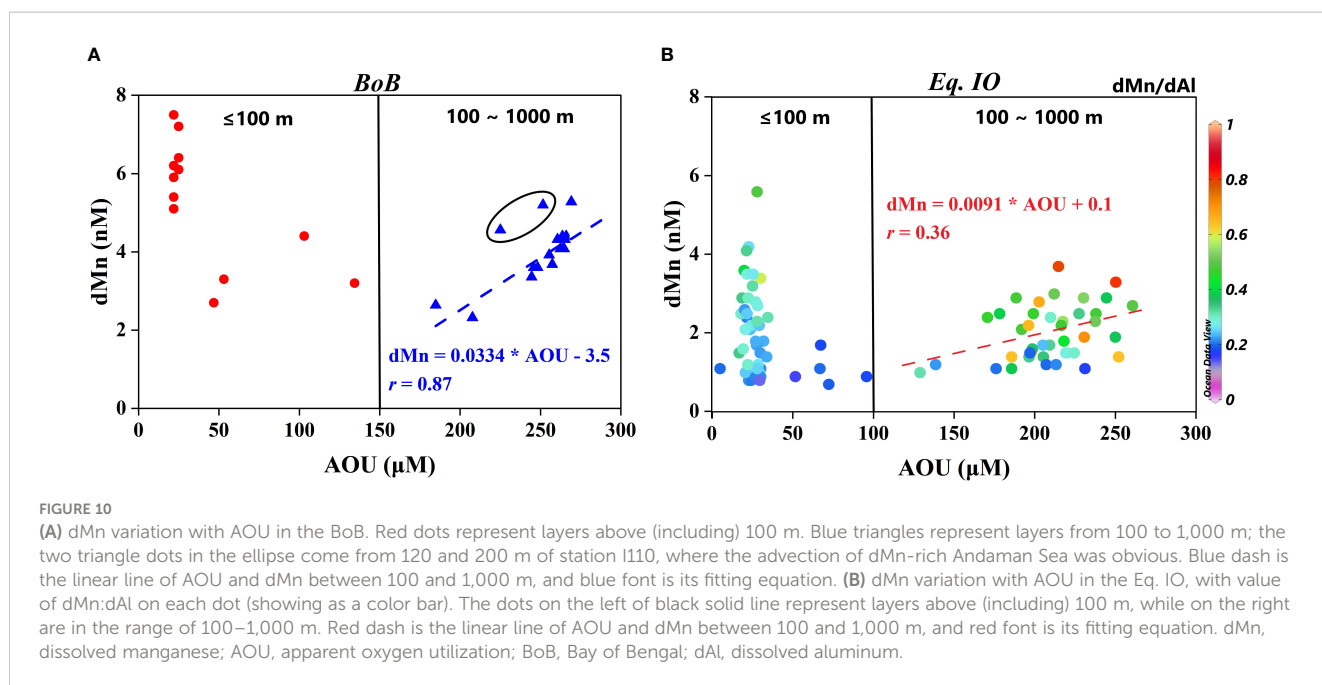
was significant for a cold-core eddy. The decrease in dAl and dMn concentrations with an increase in salinity of these two stations could be attributed to cold-core eddies pumping sub-surface water into the surface.

The Eq. IO was relatively far from the continent, where the atmospheric deposition was the main external source of dAl and dMn in the mixed layer. Substituting solubility, residence time, atmospheric dry deposition flux (36.0 mg Al·m⁻²·year⁻¹ and 936.0 μg Mn·m⁻²·year⁻¹; Srinivas and Sarin, 2013), and depth of mixed layer (30–35 m, this study) into Equation 1, atmospheric Al and Mn dry deposition to the mixed layer of the Eq. IO was calculated as 1.5–1.8 and 0.2–0.3 nM, respectively, accounting for 20%–24% dAl and 10%–14% dMn concentrations (7.4 and 2.1 nM, respectively) in the mixed layer of the Eq. IO. Atmospheric dust deposition may not play a significant role. Nevertheless, zonal distributions of dAl and dMn showed an increasing trend from west to east in section E (Figures 3C, D). Meanwhile, significantly correlated variations (Figure 8) were found between dAl, dMn, and salinity in the mixed layer of the Eq. IO (stations located in 5°S–5°N). Average values in two locations, i.e., the south BoB of this study (salinity = 33.20, dAl = 16.6 nM, dMn = 6.7 nM) and ER-8 (4.02°N, 69.00°W, salinity = 35.49, dAl = 3.0 nM, dMn = 1.4 nM, Thi Dieu Vu and Sohrin, 2013), apparently bounded the upper and lower ends of linear dAl and dMn variations with salinity in the Eq. IO region, suggesting that the dAl and dMn distributions in the surface water of the Eq. IO were predominantly controlled by the advective mixing of low-salinity, dAl-rich, and dMn-rich south BBW and relatively high-salinity, dAl-poor, and dMn-poor ASHSW.

Station I507 (6.49°S, 98.33°N) in the southeast of the study area was influenced by the ITF (5°S–15°S, You and Tomczak, 1993; Makarim et al., 2019) and possessed relatively high dAl concentrations in the upper water column (<500 m). The ITF carries 10 Sv (1 Sv = 10⁶ m³/s) low-temperature, low-salinity, oxygen-rich, and Al-rich water westward into the IO (Gordon,

2005) and can be transported to the west IO by the SEC (Grand et al., 2015a). The ITF played significant roles in governing the dAl and dMn concentrations in the surface water, especially below the surface mixed layer, where the Al and Mn release from the settling mineral particles was deemed negligible (Measures et al., 2010; Grand et al., 2015b). Elevated ²²⁸Ra activities (>100 dpm/m³; Nozaki and Yamamoto, 2001) were observed in the surface waters at PA-7 (Figure 1, 10.01°S, 103.00°E, Obata et al., 2004), where high dAl concentrations (10.0 and 9.8 nM) appeared in the mixed layer and upper water column (100–500 m), respectively, suggested that the ITF, carrying coastal and shelf sources of trace elements, may have a significant contribution to dAl and dMn in the surface waters of the east IO.

The T-S diagram (Figure 5) indicated that intermediate water (σ_θ within 27.1–27.6 kg/m³, depth in the range of 750–1,500 m) in the study area was mainly mixed by IIW and RSIW. IIW, characterized by relatively low salinity and high oxygen, largely contributes approximately 30%–50% of its water into the BoB. On the contrary, RSIW is characterized by high salinity and low oxygen and contributes approximately 40% of its water into the BoB. The main component of the intermediate water body of stations ER-5 and ER-6 from Thi Dieu Vu and Sohrin (2013) was hypothesized as the RSIW. Stations PA-2 and PA-7 from Obata et al. (2004) were on the pathway of IIW spreading northward. Both IIW and RSIW were characterized by low dAl (Obata et al., 2004; Thi Dieu Vu and Sohrin, 2013), and when moving into the BoB as a western boundary current through the east of Sri Lanka and flowed clockwise, they exited the bay, carrying high dAl and dMn concentrations (Figure 9, I205 and I106) of intermediate water of the BoB southward along Sumatra and Java (Figure 9; You, 1998). The intermediate water body of stations I103, I415, and I504 from this study and ER-3 from Thi Dieu Vu and Sohrin (2013) were considered the results of IIW and RSIW, together with BoB intermediate water body mixing, and therefore, plots for salinity



and dAl concentrations of these stations located in the dashed triangle constituted IIW, RSIW, and BoB intermediate water body (Figure 9). Based on the fact that northeastern IO is with low oxygen and that the BoB is anoxic (Figure 4B), remineralization and/or regeneration under a low-oxygen environment also mattered during the transporting of IIW and RSIW and in the subsurface water of the BoB, which will be discussed in the following section.

Remineralization versus reduction regeneration in anoxic zone

The poor ventilation of waters associated with the existence of NICW resulted in hypoxic conditions (DO below 32 μM , Figure 4B) in the subsurface and intermediate waters body of the BoB, along with high dAl and dMn concentrations simultaneously (Figures 4C, D). High or increased dAl concentration in the subsurface (100–1,000 m) was observed (Figure 4C). dAl in the depth of 100–1,000 m behaved non-conservatively with a poor relationship between dAl and salinity ($r < 0.22$, figure not shown), while dAl showed no correlation ($r < 0.24$, figure not shown) with apparent oxygen utilization (AOU) either. Singh et al. (2020) also observed the increase in dAl levels in the subsurface water and that dAl concentrations showed an overall decrease with increasing nutrients in the thermocline waters (100–800 m), and they concluded as regards the supply from the continental margin.

A tight correlation (Figure 10A, blue triangle dots, $r = 0.87$) between dMn and AOU in the subsurface water depth (100–1,000 m) of the BoB indicated that remineralization and/or regeneration mattered in regulating the biogeochemical behavior of dMn in a hypoxic environment. Two triangle dots in the ellipse came from 120 and 200 m of station I110, which could be attributed to the advection of dMn-rich Andaman Sea (Figures 2B, D), along with resuspended sediments from the margin shelf (Singh et al., 2020). AOU has been used to quantify the remineralized part of nutrients for its function as a tracer of organic matter remineralization (Anderson and Sarmiento, 1995; Chen and Wu, 2019). The slope achieved from the dMn : AOU linear relationship in this study was 0.0334 nM/ μM , which could be converted to Mn:P = 5.01 nM/ μM and Mn:C = 47.3 $\mu\text{M}/\text{M}$ by applying the most commonly used Redfield ratio AOU:P:C = 150:1:106 (Redfield, 1958; Tyrrell, 2019). These two ratios far exceed the range in phytoplankton Mn:P = 0.16–0.81 nM/ μM and Mn:C = 0.6–1.8 in $\mu\text{M}/\text{M}$ reported and summarized in Twining et al. (2010) and Twining et al. (2019), respectively. This indicated that remineralization of biogenic particulate, compared to a reduction of Mn(IV) from lithogenic particles and/or resuspended sediments from the margin in hypoxic conditions, could be deemed as negligible for the distribution of dMn in the BoB while ignoring the effects of vertical mixing.

The low DO in the subsurface of the Eq. IO was the result of NICW expanding southward and eastward and suppressed by the ITF near 5°S–10°S (Grand et al., 2015b). The relatively tight correlation ($r = 0.79$, figure not shown) between dAl and salinity in

the subsurface (100–1,000 m) of the Eq. IO suggested inconspicuous regeneration of dAl. On the contrary, the value of dMn:dAl (Figure 10B) increased nearly up to ~ 0.8 at some layers of the Eq. IO, indicating the existence of regeneration of dMn. However, a poor relationship (Figure 10B, $r = 0.36$) between dMn and AOU indicated a vague contribution of AOU under a low oxygen environment to the distribution of dMn. Similarly, no subsurface Mn maximum was observed in the oxygen minimum zone (OMZ; $< 100 \mu\text{M}$, somewhere $< 10 \mu\text{M}$) layer in the tropical and equatorial Pacific Ocean (Chen and Wu, 2019). The average AOU value in the depth of 100–500 m of the Eq. IO was 203.3 μM . Therefore, 0.2–1.1 nM of Mn was calculated by remineralization through the Redfield ratio AOU:P = 150:1 (Tyrrell, 2019) and Mn:P = 0.16–0.81 nM/ μM in the cell (Twining et al., 2010). The mean value of dMn in the subsurface (100–500 m) water of Section E in the Eq. IO was 1.8 nM (ranging from 0.8 to 3.7 nM). Therefore, the remineralization of settling organic particles contributed 11%–61% dMn in the subsurface water of the Eq. IO, which was different from that in the subsurface water of the BoB. The macronutrients and dissolved Fe were extremely low on the surface of IO tropical water, resulting in low production in the region (Wiggert et al., 2006; Grand et al., 2015b; Chinni et al., 2019). Low production in the upper water body (POC export flux (^{234}Th based): 1.0 mmol C·m²·day⁻¹; Station 10, 3.5°S, 84.0°E, Anand et al., 2017) resulted in less particle settlement and *in situ* reduction of Mn(IV) from settling, and suspended particles did not likely occur in the subsurface water body.

Conclusions

This study provided a comprehensive dataset on the distributions and sources of dissolved aluminum and manganese in the northeastern Indian Ocean in the spring inter-monsoon period of 2017. The mean values of dAl and dMn in the mixed layer of the BoB were 16.6 and 6.7 nM, respectively. The release of lithogenic sediments predominately controlled the concentration of dAl and was of great importance in dMn distributions in the mixed layer of the BoB. Additional dMn input from the advection of Andaman Sea water and photo-reduction–dissolution of particulate Mn also played significant roles. Different from that in the BoB, dAl and dMn distributions in the mixed layer of the Eq. IO were predominantly controlled by the advective mixing of low-salinity, dAl-rich, and dMn-rich south BBW and high-salinity, dAl-poor, and dMn-poor ASHSW. The intermediate water (750–1,500 m) of northeastern IO was mainly formed by the migration and mixing of low-dAl, low-dMn RSIW and IIW and BoB intermediate water characterized with high dAl and dMn concentrations. Regeneration of lithogenic particles under hypoxic conditions controlled the distribution of dMn in the subsurface (100–1,000 m) of the BoB. On the contrary, the remineralization of settling organic particles mattered in the subsurface (100–500 m) water of the Eq. IO. The influence of low salinity, dAl-rich, and dMn-rich ITF was also observed in the southernmost area of the study.

Data availability statement

The raw data supporting the conclusions of this article will be made available by the authors, without undue reservation.

Author contributions

SJ and JZ were in charge of the sampling. LL was in charge of the measurements. YY was in charge of writing/original draft preparation. JZ and JR acquired the funding for the cruise and supervised the research cruise. All authors have read and agreed to the published version of the manuscript. The manuscript was written through the contributions of all authors. All authors contributed to the article and approved the submitted version.

Funding

This study was funded by the National Natural Science Foundation of China (42176042), the High-end users Program of “Kexue” (No. KEXUE2019GZ01), and the Taishan Scholars Programme of Shandong Province. The Oceanographic Research Vessel Sharing Plan (NORC2017-10) supported by the National Natural Science Foundation of China provided precious onboard opportunities.

References

- Aguilar-Islas, A. M., and Bruland, K. W. (2006). Dissolved manganese and silicic acid in the Columbia river plume: A major source to the California current and coastal waters off Washington and Oregon. *Mar. Chem.* 101, 233–247. doi: 10.1016/j.marchem.2006.03.005
- Anand, S. S., Rengarajan, R., Sarma, V., Sudheer, A. K., Bhushan, R., and Singh, S. K. (2017). Spatial variability of upper ocean POC export in the bay of Bengal and the Indian ocean determined using particle-reactive ^{234}Th . *J. Geophys. Res.* 122, 3753–3770. doi: 10.1002/2016JC012639
- Anderson, L. A., and Sarmiento, J. L. (1995). Global ocean phosphate and oxygen simulations. *Glob. Biogeochem. Cycle* 9, 621–636. doi: 10.1029/95GB01902
- Baker, A. R., Jickells, T. D., Witt, M., and Linge, K. L. (2006). Trends in the solubility of iron, aluminium, manganese and phosphorus in aerosol collected over the Atlantic ocean. *Mar. Chem.* 98, 43–58. doi: 10.1016/j.marchem.2005.06.004
- Behrenfeld, M. J., and Falkowski, P. G. (1997). Photosynthetic rates derived from satellite-based chlorophyll concentration. *Limnol. Oceanogr.* 42, 1–20. doi: 10.4319/lo.1997.42.1.0001
- Brown, M. T., and Bruland, K. W. (2008). An improved flow injection analysis method for the determination of dissolved aluminum in seawater. *Limnol. Oceanogr. Methods* 6, 87–95. doi: 10.4319/lom.2008.6.87
- Bruland, K. W., Middag, R., and Lohan, M. C. (2014). “Controls of trace metals in seawater,” in *Treatise on geochemistry*, 2nd ed., (Oxford: Elsevier) vol. 8., 19–51.
- Buck, C. S., Landing, W. M., and Resing, J. (2013). Pacific ocean aerosols: Deposition and solubility of iron, aluminum, and other trace elements. *Mar. Chem.* 157, 117–130. doi: 10.1016/j.marchem.2013.09.005
- Chen, G., and Wu, J. (2019). Meridional distribution of dissolved manganese in the tropical and equatorial pacific. *Geochim. Cosmochim. Acta* 263, 50–67. doi: 10.1016/j.gca.2019.06.048
- Chinni, V., Singh, S. K., Bhushan, R., Rengarajan, R., and Sarma, V. V. S. S. (2019). Spatial variability in dissolved iron concentrations in the marginal and open waters of the Indian ocean. *Mar. Chem.* 208, 11–28. doi: 10.1016/j.marchem.2018.11.007
- Colombo, M., Jackson, S. L., Cullen, J. T., and Orians, K. J. (2020). Dissolved iron and manganese in the Canadian Arctic ocean: On the biogeochemical processes controlling their distributions. *Geochim. Cosmochim. Acta* 277, 150–174. doi: 10.1016/j.gca.2020.03.012

Acknowledgments

Crews and captains of *R/V ShiYan 3* are acknowledged for their help during the fieldwork. R. Schlitzer and colleagues from the Alfred Wegener Institute for Polar and Marine Research (AWI) provided free use of the software Ocean Data View (ODV), which was used for data processing. The data for this study are available from the corresponding author via email: renjingl@ouc.edu.cn.

Conflict of interest

The authors declare that the research was conducted in the absence of any commercial or financial relationships that could be construed as a potential conflict of interest.

Publisher's note

All claims expressed in this article are solely those of the authors and do not necessarily represent those of their affiliated organizations, or those of the publisher, the editors and the reviewers. Any product that may be evaluated in this article, or claim that may be made by its manufacturer, is not guaranteed or endorsed by the publisher.

- Colombo, M., Li, J., Rogalla, B., Allen, S. E., and Maldonado, M. T. (2022). Particulate trace element distributions along the Canadian Arctic GEOTRACES section: Shelf-water interactions, advective transport and contrasting biological production. *Geochim. Cosmochim. Acta* 323, 183–201. doi: 10.1016/j.gca.2022.02.013
- Dai, A., and Trenberth, K. (2002). Estimates of freshwater discharge from continents: Latitudinal and seasonal variations. *J. Hydrometeorol.* 3, 660–685. doi: 10.1175/1525-7541(2002)003<0660:EOFDFC>2.0.CO;2
- ESR (2009). OSCAR third degree resolution ocean surface currents. *Ver. 1. PO.DAAC, CA, USA*. Dataset accessed [2021-04-20] at . doi: 10.5067/OSCAR-03D01
- Galy, A., and France-Lanord, C. (2001). Higher erosion rates in the Himalaya: Geochemical constraints on riverine fluxes. *Geology (Boulder)* 29, 23. doi: 10.1130/0091-7613(2001)029<0023:HERITH>2.0.CO;2
- GEOTRACES Planning Group (2006). *GEOTRACES science plan* (Baltimore, Maryland: Scientific Committee on Oceanic Research).
- Gerringa, L. J. A., Alderkamp, A., van Dijken, G., Laan, P., Middag, R., and Arrigo, K. R. (2020). Dissolved trace metals in the Ross Sea. *Front. Mar. Sci.* 7. doi: 10.3389/fmars.2020.577098
- Gordon, A. (2005). Oceanography of the Indonesian seas and their throughflow. *Oceanography (Washington D.C.)* 18, 14–27. doi: 10.5670/oceanog.2005.01
- Grand, M. M., Measures, C. I., Hatta, M., Hiscock, W. T., Buck, C. S., and Landing, W. M. (2015a). Dust deposition in the eastern Indian ocean: The ocean perspective from Antarctica to the bay of Bengal. *Glob. Biogeochem. Cycle* 29, 357–374. doi: 10.1002/2014GB004898
- Grand, M. M., Measures, C. I., Hatta, M., Hiscock, W. T., Landing, W. M., Morton, P. L., et al. (2015b). Dissolved Fe and Al in the upper 1000 m of the eastern Indian ocean: A high-resolution transect along 95°E from the Antarctic margin to the bay of Bengal. *Glob. Biogeochem. Cycle* 29, 375–396. doi: 10.1002/2014GB004920
- Häusler, K., Dellwig, O., Schnetger, B., Feldens, P., Leipe, T., Moros, M., et al. (2018). Massive Mn carbonate formation in the land sort deep (Baltic sea): Hydrographic conditions, temporal succession, and Mn budget calculations. *Mar. Geol.* 395, 260–270. doi: 10.1016/j.margeo.2017.10.010
- Holte, J., Talley, L. D., Gilson, J., and Roemmich, D. (2017). An argo mixed layer climatology and database. *Geophys. Res. Lett.* 44, 5618–5626. doi: 10.1002/2017GL073426

- Hood, R. R., Wiggert, J. D., and Naqvi, S. W. A. (2009). Indian Ocean research: Opportunities and challenges. *Geophysical Monograph Ser.* 185, 409–429. doi: 10.1029/2007GM000714
- Hsu, S., Wong, G. T. F., Gong, G., Shiah, F., Huang, Y., Kao, S., et al. (2010). Sources, solubility, and dry deposition of aerosol trace elements over the East China Sea. *Mar. Chem.* 120, 116–127. doi: 10.1016/j.marchem.2008.10.003
- Jian, J., Webster, P. J., and Hoyos, C. D. (2009). Large-Scale controls on Ganges and Brahmaputra river discharge on intraseasonal and seasonal time-scales. *Q. J. R. Meteorol. Soc.* 135, 353–370. doi: 10.1002/qj.384
- Kadko, D., Aguilar-Islas, A., Buck, C. S., Fitzsimmons, J. N., Landing, W. M., Shiller, A., et al. (2020). Sources, fluxes and residence times of trace elements measured during the U.S. GEOTRACES East Pacific zonal transect. *Mar. Chem.* 222, 103781. doi: 10.1016/j.marchem.2020.103781
- Kamykowski, D., and Zentara, S. (1990). Hypoxia in the world ocean as recorded in the historical data set. *Deep Sea Res. Part I* 37, 1861–1874. doi: 10.1016/0198-0149(90)90082-7
- Kandel, A., and Aguilar-Islas, A. (2021). Spatial and temporal variability of dissolved aluminum and manganese in surface waters of the northern gulf of Alaska. *Deep Sea Res. Part II* 189–190, 104952. doi: 10.1016/j.dsr2.2021.104952
- Landing, W. M., and Bruland, K. W. (1980). Manganese in the north Pacific. *Earth Planet. Sci. Lett.* 49, 45–56. doi: 10.1016/0012-821X(80)90149-1
- Lee, J., Heller, M. I., and Lam, P. J. (2018). Size distribution of particulate trace elements in the U.S. GEOTRACES Eastern Pacific zonal transect (GP16). *Mar. Chem.* 201, 108–123. doi: 10.1016/j.marchem.2017.09.006
- Lenstra, W. K., Séguet, M. J. M., Behrends, T., Groeneveld, R. K., Hermans, M., Witbaard, R., et al. (2020). Controls on the shuttling of manganese over the northwestern black Sea shelf and its fate in the euxinic deep basin. *Geochim. Cosmochim. Acta* 273, 177–204. doi: 10.1016/j.gca.2020.01.031
- Lewis, B. L., and Luther III, G. W. (2000). Processes controlling the distribution and cycling of manganese in the oxygen minimum zone of the Arabian Sea. *Deep-sea research. Part II, Tropical studies in oceanography* 47, 1541–1561. doi: 10.1016/S0967-0645(99)00153-8
- López-García, P., Gelado-Caballero, M. D., Collado-Sánchez, C., and Hernández-Brito, J. J. (2017). Solubility of aerosol trace elements: Sources and deposition fluxes in the canary region. *Atmos. Environ.* 148, 167–174. doi: 10.1016/j.atmosenv.2016.10.035
- Makarim, S., Sprintall, J., Liu, Z., Yu, W., Santoso, A., Yan, X., et al. (2019). Previously unidentified Indonesian throughflow pathways and freshening in the Indian ocean during recent decades. *Sci. Rep.* 9, 7364. doi: 10.1038/s41598-019-43841-z
- Martin, J. H., and Knauer, G. A. (1980). Manganese cycling in northeast Pacific waters. *Earth Planet. Sci. Lett.* 51, 266–274. doi: 10.1016/0012-821X(80)90209-5
- Measures, C. I., and Brown, E. T. (1996). “Estimating dust input to the Atlantic ocean using surface water aluminium concentrations,” in *The impact of desert dust across the Mediterranean*. Eds. S. Guerzoni and R. Chester (Dordrecht: Springer Netherlands), 301–311.
- Measures, C. I., and Edmond, J. M. (1990). Aluminium in the south Atlantic: Steady state distribution of a short residence time element. *J. Geophys. Res. Oceans*. 95, 5331–5340. doi: 10.1029/JC095iC04p05331
- Measures, C. I., Sato, T., Vink, S., Howell, S., and Li, Y. H. (2010). The fractional solubility of aluminium from mineral aerosols collected in Hawaii and implications for atmospheric deposition of biogeochemically important trace elements. *Mar. Chem.* 120, 144–153. doi: 10.1016/j.marchem.2009.01.014
- Menzel Barraqueta, J., Samanta, S., Achterberg, E. P., Bowie, A. R., Croot, P., Cloete, R., et al. (2020). A first global oceanic compilation of observational dissolved aluminum data with regional statistical data treatment. *Front. Mar. Sci.* 7. doi: 10.3389/fmars.2020.00468
- Menzel Barraqueta, J., Schlosser, C., Planquette, H., Gourain, A., Cheize, M., Boutorh, J., et al. (2018). Aluminium in the north Atlantic ocean and the Labrador Sea (GEOTRACES GA01 section): Roles of continental inputs and biogenic particle removal. *Biogeosciences* 15, 5271–5286. doi: 10.5194/bg-15-5271-2018
- Nakaguchi, Y., Ikeda, Y., Sakamoto, A., Zheng, L., Minami, T., and Sohrin, Y. (2021). Distribution and stoichiometry of Al, Mn, Fe, Co, Ni, Cu, Zn, Cd, and Pb in the East China Sea. *J. Oceanogr.* 77, 463–485. doi: 10.1007/s10872-020-00577-z
- Nath, B. N., Rao, V. P., and Becker, K. P. (1989). Geochemical evidence of terrigenous influence in deep-sea sediments up to 8°S in the central Indian basin. *Mar. Geol.* 87, 301–313. doi: 10.1016/0025-3227(89)90067-4
- Nozaki, Y., and Yamamoto, Y. (2001). Radium 228 based nitrate fluxes in the eastern Indian ocean and the south China Sea and a silicon-induced “alkalinity pump” hypothesis. *Glob. Biogeochem. Cycle* 15, 555–567. doi: 10.1029/2000GB001309
- Obata, H., Nozaki, Y., Alibo, D. S., and Yamamoto, Y. (2004). Dissolved Al, in, and ce in the eastern Indian ocean and the southeast Asian seas in comparison with the radionuclides 210Pb and 210Po. *Geochim. Cosmochim. Acta* 68, 1035–1048. doi: 10.1016/j.gca.2003.07.021
- Redfield, A. C. (1958). The biological control of chemical factors in the environment. *Am. Sci.* 46, 221A–230A. Available at: <http://www.jstor.org/stable/27827150>
- Resing, J. A., Sedwick, P. N., German, C. R., Jenkins, W. J., Moffett, J. W., Soht, B. M., et al. (2015). Basin-scale transport of hydrothermal dissolved metals across the south Pacific ocean. *Nature* 523, 200–203. doi: 10.1038/nature14577
- Rolison, J. M., Middag, R., Stirling, C. H., Rijkenberg, M. J. A., and de Baar, H. J. W. (2015). Zonal distribution of dissolved aluminium in the Mediterranean Sea. *Mar. Chem.* 177, 87–100. doi: 10.1016/j.marchem.2015.05.001
- Sandeep, K. K., Pant, V., Girishkumar, M. S., and Rao, A. D. (2018). Impact of riverine freshwater forcing on the sea surface salinity simulations in the Indian ocean. *J. Mar. Syst.* 185, 40–58. doi: 10.1016/j.jmarsys.2018.05.002
- Sardessai, S., Shetye, S., Maya, M. V., Mangala, K. R., and Prasanna Kumar, S. (2010). Nutrient characteristics of water masses and their seasonal variability in the eastern equatorial Indian Ocean. *Mar. Environ. Res.* 70, 272–282. doi: 10.1016/j.marenvres.2010.05.009
- Schott, F. A., Xie, S., and Julian, P. M. J. (2009). Indian Ocean circulation and climate variability. *Rev. Geophys.* 1985) 47, G1002. doi: 10.1029/2007RG000245
- Sengupta, D., Bharath Raj, G. N., and Sheno, S. S. C. (2006). Surface freshwater from bay of Bengal runoff and Indonesian throughflow in the tropical Indian ocean. *Geophys. Res. Lett.* 33. doi: 10.1029/2006GL027573
- Shankar, D., Vinayachandran, P. N., and Unnikrishnan, A. S. (2002). The monsoon currents in the north Indian ocean. *Prog. Oceanogr.* 52, 63–120. doi: 10.1016/s0079-6611(02)00024-1
- Shiller, A. M. (1997). Manganese in surface waters of the Atlantic ocean. *Geophys. Res. Lett.* 24, 1495–1498. doi: 10.1029/97GL01456
- Singh, N. D., Chinni, V., and Singh, S. K. (2020). Dissolved aluminium cycling in the northern, equatorial and subtropical gyre region of the Indian ocean. *Geochim. Cosmochim. Acta* 268, 160–185. doi: 10.1016/j.gca.2019.09.028
- Singh, S. K., and France-Lanord, C. (2002). Tracing the distribution of erosion in the Brahmaputra watershed from isotopic compositions of stream sediments. *Earth Planet. Sci. Lett.* 202, 645–662. doi: 10.1016/s0012-821x(02)00822-1
- Singh, N. D., and Singh, S. K. (2022). Distribution and cycling of dissolved aluminium in the Arabian Sea and the Western equatorial Indian ocean. *Mar. Chem.* 243, 104122. doi: 10.1016/j.marchem.2022.104122
- Singh, S. P., Singh, S. K., Goswami, V., Bhushan, R., and Rai, V. K. (2012). Spatial distribution of dissolved neodymium and eNd in the bay of Bengal: Role of particulate matter and mixing of water masses. *Geochim. Cosmochim. Acta* 94, 38–56. doi: 10.1016/j.gca.2012.07.017
- Slemons, L. O., Murray, J. W., Resing, J., Paul, B., and Dutrieux, P. (2010). Western Pacific coastal sources of iron, manganese, and aluminum to the equatorial undercurrent. *glob. Biogeochem. Cycle* 24, GB3024-1–GB3024-16. doi: 10.1029/2009GB003693
- Srinivas, B., and Sarin, M. M. (2013). Atmospheric dry-deposition of mineral dust and anthropogenic trace metals to the bay of Bengal. *J. Mar. Syst.* 126, 56–68. doi: 10.1016/j.jmarsys.2012.11.004
- Srinivas, B., Sarin, M. M., and Kumar, A. (2012). Impact of anthropogenic sources on aerosol iron solubility over the bay of Bengal and the Arabian Sea. *Biogeochemistry* 110, 257–268. doi: 10.1007/s10533-011-9680-1
- Statham, P. J., Yeats, P. A., and Landing, W. M. (1998). Manganese in the eastern Atlantic ocean: Processes influencing deep and surface water distributions. *Mar. Chem.* 61, 55–68. doi: 10.1016/S0304-4203(98)00007-3
- Sunda, W. G., and Huntsman, S. A. (1988). Effect of sunlight on redox cycles of manganese in the southwestern Sargasso Sea. *Deep Sea Res. Part I* 35, 1297–1317. doi: 10.1016/0198-0149(88)90084-2
- Sunda, W. G., and Huntsman, S. A. (1994). Photoreduction of manganese oxides in seawater. *Mar. Chem.* 46, 133–152. doi: 10.1016/0304-4203(94)90051-5
- Taylor, S. R., and McLennan, S. M. (1985). *The continental crust: Its composition and evolution, an examination of the geochemical record preserved in sedimentary rocks* (Oxford: Blackwell Scientific Pub).
- Tessier, A., Campbell, P. G. C., and Bisson, M. (1979). Sequential extraction procedure for the speciation of particulate trace metals. *Analytical Chem. (Washington)* 51, 844–851. doi: 10.1021/ac50043a017
- Thi Dieu Vu, H., and Sohrin, Y. (2013). Diverse stoichiometry of dissolved trace metals in the Indian ocean. *Sci. Rep.* 3, 1745. doi: 10.1038/srep01745
- Twining, B. S., Nuez-Milland, D., Vogt, S., Johnson, R. S., and Sedwick, P. N. (2010). Variations in synechococcus cell quotas of phosphorus, sulfur, manganese, iron, nickel, and zinc within mesoscale eddies in the Sargasso Sea. *Limnol. Oceanogr.* 55, 492–506. doi: 10.4319/lo.2010.55.2.0492
- Twining, B. S., Rauschenberg, S., Baer, S. E., Lomas, M. W., Martiny, A. C., and Antipova, O. (2019). A nutrient limitation mosaic in the eastern tropical Indian ocean. *Deep Sea Res. Part II* 166, 125–140. doi: 10.1016/j.dsr2.2019.05.001
- Tyrell, T. (2019). “Redfield ratio,” in *Encyclopedia of ocean sciences (Third edition)*, (Oxford: Elsevier) vol. 1, 461–472.
- Unger, D., Tttekkot, V., Schäfer, P., Tiemann, J., and Reschke, S. (2003). Seasonality and interannual variability of particle fluxes to the deep bay of Bengal: Influence of riverine input and oceanographic processes. *Deep Sea Res. Part II* 50, 897–923. doi: 10.1016/s0967-0645(02)00612-4
- Wang, Z., Ren, J., Xuan, J., Li, F., Yang, T., and Guo, Y. (2018). Processes controlling the distribution and cycling of dissolved manganese in the northern south China Sea. *Mar. Chem.* 204, 152–162. doi: 10.1016/j.marchem.2018.07.003
- Wiggert, J. D., Murtugudde, R. G., and Christian, J. R. (2006). Annual ecosystem variability in the tropical Indian ocean: Results of a coupled bio-physical ocean general circulation model. *Deep Sea Res. Part II* 53, 644–676. doi: 10.1016/j.dsr2.2006.01.027

- You, Y. (2000). Implications of the deep circulation and ventilation of the Indian Ocean on the renewal mechanism of North Atlantic Deep Water. *Journal of Geophysical Research: Ocean* 105, 23895–23926. doi: 10.1029/2000JC900105
- You, Y. (1997). Seasonal variations of thermocline circulation and ventilation in the Indian ocean. *J. Geophys. Res. Oceans*. 102, 10391–10422. doi: 10.1029/96JC03600
- You, Y. (1998). Intermediate water circulation and ventilation of the Indian ocean derived from water-mass contributions. *J. Mar. Res.* 56, 1029–1067. doi: 10.1357/002224098765173455
- You, Y., and Tomczak, M. (1993). Thermocline circulation and ventilation in the Indian ocean derived from water mass analysis. *Deep Sea Res. Part I* 40, 13–56. doi: 10.1016/0967-0637(93)90052-5
- Zhang, R., John, S. G., Zhang, J., Ren, J., Wu, Y., Zhu, Z., et al. (2015a). Transport and reaction of iron and iron stable isotopes in glacial meltwaters on Svalbard near kongsfjorden: From rivers to estuary to ocean. *Earth Planet. Sci. Lett.* 424, 201–211. doi: 10.1016/j.epsl.2015.05.031
- Zhang, R., Zhang, J., Ren, J., Li, J., Li, F., Wang, Z., et al. (2015b). X-Vane: A sampling assembly combining a niskin-X bottle and titanium frame vane for trace metal analysis of sea water. *Mar. Chem.* 177, 653–661. doi: 10.1016/j.marchem.2015.10.006
- Zheng, L., Minami, T., Takano, S., and Sohrin, Y. (2022). Distributions of aluminum, manganese, cobalt, and lead in the western south pacific: Interplay between the south and north pacific. *Geochim. Cosmochim. Acta* 338, 105–120. doi: 10.1016/j.gca.2022.10.022